Intrinsic Conductivity in Sodium−Air Battery Discharge Phases: Sodium Superoxide vs Sodium Peroxide
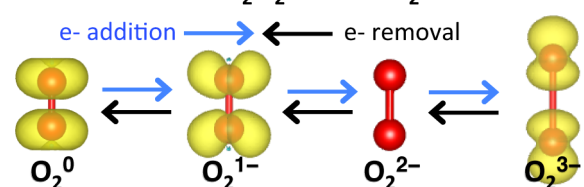
Sheng Yang[†] and Donald J. Siegel*[,‡,§]

[†]Department of Physics, [‡]Mechanical Engineering Department, and [§]Applied Physics Program, University of Michigan, Ann Arbor, Michigan 48109, United States

Ⓢ *Supporting Information*

ABSTRACT: The primary discharge product in sodium−air batteries has been reported in some experiments to be sodium peroxide, Na_2O_2, while in others sodium superoxide, NaO_2, is observed. Importantly, cells that discharge to NaO_2 exhibit low charging overpotentials, while those that discharge to Na_2O_2 do not. These differences could arise from a higher conductivity within the superoxide; however, this explanation remains speculative given that charge transport in superoxides is relatively unexplored. Here, density functional and quasi-particle GW methods are used to comparatively assess the conductivities of

Magnetization and charge state for O_2 dimers in Na_2O_2 and NaO_2

e- addition → ← e- removal

O_2^0 O_2^{1-} O_2^{2-} O_2^{3-}

Na−O_2 discharge phases by calculating the concentrations and mobilities of intrinsic charge carriers in Na_2O_2 and NaO_2. Both compounds are predicted to be electrical insulators, with bandgaps in excess of 5 eV. In the case of sodium peroxide, the transport properties are similar to those reported previously for lithium peroxide, suggesting low bulk conductivity. Transport in the superoxide has some features in common with the peroxide but also differs in important ways. Similar to Na_2O_2, NaO_2 is predicted to be a poor electrical conductor, wherein transport is limited by sluggish charge hopping between O_2 dimers. Different from Na_2O_2, in NaO_2 this transport is mediated by a combination of electron and hole polarons. An additional distinguishing feature of the superoxide is its ionic conductivity, which is 10 orders of magnitude larger than the electronic component. The ionic component is comprised primarily of p-type contributions from (surprisingly mobile) oxygen dimer vacancies, and from n-type contributions from negative sodium vacancies. In the context of sodium−air batteries, the low electronic conductivity afforded by NaO_2 suggests that enhanced bulk transport within this phase is unlikely to account for the low overpotentials associated with its decomposition. Rather, the enhanced efficiency of NaO_2-based cells should be attributed to other factors, such as a reduced tendency for electrolyte decomposition.

1. INTRODUCTION

Nonaqueous metal−air batteries are attracting increasing attention as a future energy storage technology. For example, the Li−O_2 battery, one of the most extensively studied metal−oxygen systems, exhibits a theoretical specific energy which is approximately 8 times higher than that of Li-ion batteries (LIBs).[1] However, Li−O_2 batteries suffer from poor cycle life and low round-trip efficiency, the latter effect arising from high overpotentials during charging.[2−5]

As an alternative to lithium-based chemistries, recent experiments have probed the performance of Na−O_2 batteries.[6−10] Although Na and Li are both alkali metals, with Na located one row below lithium in the periodic table, the performance of Na−O_2 batteries appears to be very different from that of the analogous Li−O_2 system. For example, in Na−O_2 cells employing nonaqueous electrolytes, some studies have reported Na_2O_2 as the main discharge product,[7] while others report NaO_2.[6,8] Cells that discharge to Na_2O_2 exhibit high charging overpotentials, similar to those observed in Li−O_2 batteries. On the other hand, cells that discharge to NaO_2 have much lower charging overpotentials, typically less than 200 meV.[6,8,10]

While the greater mass of sodium implies that a Na−O_2 cell would exhibit approximately 50% lower specific energy compared to a Li-based cell, the surprising discovery of low overpotentials in superoxide-based Na−O_2 cells suggests an important battery design strategy. That is, by stabilizing a solid superoxide discharge phase it may be possible to reduce overpotentials for the oxygen evolution reaction (OER) and thereby improve round-trip efficiency. In principle, this strategy could be applied not only for the Na−O_2 system but also for Li-based and other metal−oxygen systems. In this regard the Na−O_2 chemistry serves as an important prototype for understanding the connection between the composition of the discharge product and battery efficiency.

Before applying such a strategy it would be helpful to identify which property of the superoxide phase is responsible for its low OER overpotential.[10−13] One possibility is that this behavior arises from a higher conductivity relative to the peroxide. Along these lines, Hartmann et al.[11] and Zhao et al.[10]
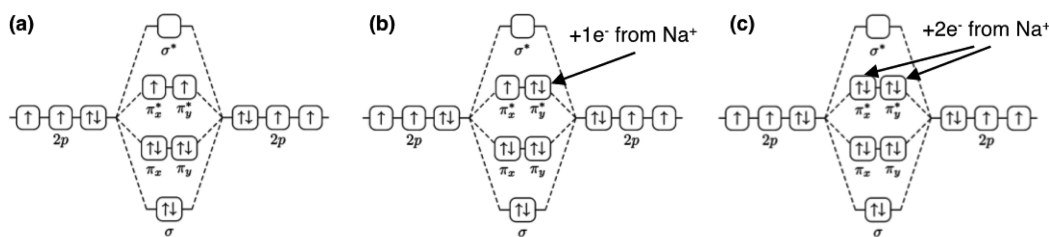
Figure 1. Molecular orbital (MO) diagrams for (a) oxygen (O_2^0), (b) superoxide (O_2^{1-}), and (c) peroxide (O_2^{2-}) dimers.

argued that the large particle sizes typical of the NaO_2 phase observed in discharged $Na-O_2$ cells implied a higher conductivity. This would be consistent with an early report that found moderate conductivity in KO_2 (approximately 1−10 S/cm).[14] More recent experiments measured the total (electronic + ionic) conductivity of KO_2 at elevated temperatures (345−500 K). Extrapolating these data to 300 K yields a much lower value of 10^{-13} S/cm.[15,16]

While the popularity of $Li-O_2$ batteries has recently sparked interest in the properties of Li_2O_2,[17−19] transport in superoxide phases has received less attention.[14−16] In the case of Li_2O_2, a small number of studies have predicted that both holes and electrons become self-trapped on oxygen dimers, forming small hole/electron polarons.[17−21] DFT+U calculations by Garcia-Lastra et al. revealed that hole polarons have a much higher mobility than do electron polarons in Li_2O_2.[17] Radin and Siegel used a tuned hybrid functional to estimate the intrinsic conductivity of Li_2O_2 by combining the calculated concentrations of various charge-carrying point defects with their respective mobilities.[18] They identified hole polarons and negative lithium vacancies as the dominant charge carriers; the low concentrations and limited mobility of these species result in the low conductivity of Li_2O_2. This result was corroborated by experiments,[22] which found the same charge-carrying species in bulk Li_2O_2. To our knowledge, much less effort has been devoted to examining intrinsic conductivity in the $Na-O$ system.[15,23]

In the present study first-principles calculations are used to predict the intrinsic conductivities of bulk Na_2O_2 and NaO_2. More specifically, the formation energies and concentrations of various charge-carrying point defects with different charge states—polarons, vacancies, and interstitials—are evaluated. Subsequent calculations assess the mobilities of the highest-concentration charge carriers. Many-body perturbation theory (GW) reveals that both Na_2O_2 and NaO_2 are wide gap insulators with bandgaps of 6.65 and 5.30 eV, respectively. Similar to earlier studies on Li_2O_2,[18,19] hole polarons (localized on O_2 dimers) and negative sodium vacancies are identified as the main charge carriers in Na_2O_2. Combining the concentration and mobility data, we find that the electronic and ionic conductivity of Na_2O_2 is essentially the same as that for Li_2O_2.

Transport phenomena are more complex in the case of the superoxide. Regarding electronic transport, our calculations predict that both electron and hole polarons contribute to the intrinsic conductivity of NaO_2 in roughly equal proportions. Although electron polarons are present in higher concentrations compared to holes, the trend in mobilities is reversed, with holes having lower hopping barriers. Ionic conductivity in NaO_2 is mediated by a mixture of negative sodium vacancies and positive oxygen dimer vacancies. Combining concentration and mobility data, our calculations find that the electronic conductivity of NaO_2 is only slightly higher than in the

peroxide and remains low in an absolute sense. This behavior differs markedly from the ionic conductivity, which is approximately 10 orders of magnitude higher in NaO_2 than in the peroxide.

These data reveal that long-range electronic transport in alkali peroxides and superoxides is governed by the unusual ability of oxygen dimers to adopt three distinct charge states: O_2^{2-}, O_2^{1-}, and O_2^0, Figure 1. More importantly, the modest electronic conductivity afforded by the superoxide suggests that enhanced bulk transport through this phase is unlikely to account for the low overpotentials associated with its decomposition. We therefore speculate that the improved performance of NaO_2-based cells arises from a reduction in the extent of side reactions, such as electrolyte decomposition.[8]

2. METHODOLOGY

Density functional theory (DFT) calculations were performed with the Vienna ab initio simulation package (VASP).[24−27] A Γ-centered K-point grid with density 4 × 4 × 6 (6 × 6 × 6) for Na_2O_2 (NaO_2) was used for calculations involving primitive cells. A 144 atom supercell generated from a 2 × 2 × 3 replication of the unit cell was used for defect calculations on Na_2O_2; a 2 × 2 × 2 supercell (96-atoms) was used for NaO_2. The Γ point was used for defect calculations involving supercells. All of the calculations were spin-polarized and used a planewave cutoff energy of 460 eV. For structure optimizations, all ions were relaxed to a force tolerance of 0.02 eV/Å or less. A ferromagnetic configuration was employed for NaO_2 ($Pa\overline{3}$) bulk calculations. We found this configuration to 15 meV/formula unit more stable than an antiferromagnetic state with spins that alternate on [002] planes. The magnetic state obtained from supercell calculations involving NaO_2 was observed to be consistent with that of the superoxide unit cell.

Given that semilocal functionals may poorly describe some aspects of alkali-metal superoxides and peroxides,[28,29] our calculations employ hybrid functionals based on the HSE formulation[30,31] and many-body perturbation (GW) methods,[32] in addition to the PBE generalized gradient approximation (PBE-GGA).[33] In the HSE functional the exchange potential is separated into long-range and short-range portions; the long-range portion is based on PBE exchange, while the short-range component is a mixture of Hartree−Fock exchange and PBE exchange. The mixing parameter α controls the fraction of Hartree−Fock exchange included. As shown in previous studies, hopping barriers associated with electrons and holes can be sensitive to the choice of the mixing parameter α (and, similarly to the value of U used in in GGA+U calculations).[17,18] Based on our earlier work in which we examined in detail the impact of the mixing parameter on formation energies and migration barriers,[18] in the present study we adopt the value $\alpha = 0.48$. This value reproduces the quasi-particle bandgap for Li_2O_2 and allows consistent comparisons to be made between the present calculations on Na-based phases and prior studies involving Li_2O_2.

Defect Concentration. At equilibrium and in the dilute limit, the concentration C of a point defect in a crystal can be expressed in terms of its formation energy:

$$C = N_{sites}e^{-E_f/k_BT} \quad (1)$$

where N_{sites} is the number of sites in the crystal where the defect can occur and E_f corresponds to the formation energy of a given defect. Similarly, the formation energy of a defect X^q in charge stage q is given by

$$E_f(X^q) = E_0(X^q) - E_0(\text{pristine}) - \sum_i n_i \mu_i + q\varepsilon_F + E_{MPI} \qquad (2)$$

where $E_0(X^q)$ represents the total energy of the supercell containing a defect X^q, $E_0(\text{pristine})$ is the total energy of the supercell without a defect, n_i is the number of atoms of species i, μ_i is the chemical potential of species i, ε_F is the Fermi level referenced to the valence-band maximum (VBM) in the bulk, and E_{MPI} is the Makov–Payne monopole finite-size correction.[34] The calculated dielectric constants for Na_2O_2 and NaO_2, which are needed as input to the monopole correction, are presented in the Supporting Information.

The chemical potential of oxygen in $Na-O_2$ condensed phases is assumed be fixed by equilibrium with oxygen gas at $T = 300$ K and $P = 1$ atm, while the chemical potential of sodium in Na_2O_2 or NaO_2 is expressed according to

$$\mu_{Na}(Na_2O_2) = 1/2[G(Na_2O_2) - 2\mu_o]$$

$$\mu_{Na}(NaO_2) = G(NaO_2) - 2\mu_o$$

For solid phases, we take the free energy to be the DFT ground state energy. The chemical potential of oxygen is calculated using

$$G(O_2) = E_0(O_2) + k_BT - TS_{expt} + E_{corr}$$

Here, we take $PV \approx k_BT$ and S_{expt} is the experimental entropy of oxygen gas. To account for oxygen overbinding, we correct the ground state of O_2 (E_{corr}) using the experimental formation enthalpy of Na_2O_2 and NaO_2. This raises the energy of O_2 by 0.62 and 0.10 eV, respectively. Additional details regarding the calculated thermodynamics of these phases are presented in the Supporting Information.

Defect Mobility. The conductivity associated with a given intrinsic defect depends upon its concentration and mobility. Defect mobilities, μ, are calculated using the Nernst–Einstein equation, $D = \mu k_BT/e$. Here, D is the diffusion coefficient, which is expressed as $D = \nu a^2 e^{-E_b/k_BT}$; ν is the hopping attempt frequency, which we take to be equal to the value typically used in semiconductors, 10^{13} s^{-1}.[17,18,21] The jump distance is given by a, and E_b is the diffusion barrier (neglecting entropy contributions). Inserting the expression for the diffusion coefficient, the mobility can therefore be expressed as

$$\mu = \frac{\nu e a^2}{k_BT} e^{-E_b/k_BT} \qquad (3)$$

The nudged elastic band method (NEB)[35] with the HSE$_\alpha$ functional was used to evaluate energy barriers associated with defect migration. Ionic diffusion barriers were converged to a tolerance of 0.02 eV/Å. For polaron hopping barriers, the climbing image NEB (CI-NEB) was also used.[36] In this case convergence was found to be somewhat slower. Calculations for a given hopping mechanism were run for more than 200 iterations; in the case of NaO_2 the energy barrier changed by less than 10 meV between iterations 150 and 200.

3. RESULTS AND DISCUSSION

Structure and Bandgaps. Na_2O_2 is reported to adopt an hexagonal crystal structure (space group ($P\bar{6}2m$) with lattice constants $a = 6.21$ Å and $c = 4.47$ Å.[37] The calculated lattice parameters are $a = 6.11$ Å and $c = 4.42$ Å (HSE06), in satisfactory agreement with the experimental values. Sodium cations in the peroxide structure reside in distorted trigonal prism sites, with oxygen forming the prism vertices (Figure 2a). Na_2O_2 units exhibit an ···ABAB··· stacking sequence along the c-axis: each layer has the same density of Na atoms; however, the oxygen density exhibits a higher value in "A" layers ("oxygen-rich" layer, with an O–O bond length of 1.49 Å) than
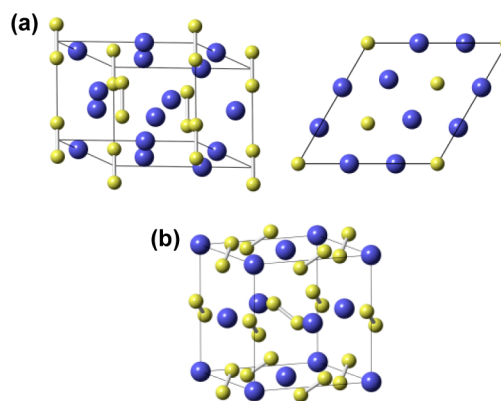
Figure 2. Crystal structures of (a) hexagonal Na_2O_2 viewed along two directions and (b) cubic (pyrite) NaO_2. Yellow spheres represent oxygen atoms; blue spheres are sodium atoms.

in "B" layers ("oxygen-poor" layer, with O–O bond length of 1.48 Å).

The NaO_2 phase exhibits several polymorphs.[38] The stable structure below 196 K is tetragonal (space group $Pnnm$); from 196 to 223 K the $Pa\bar{3}$ (NaCl rock salt structure type) is the stable phase, wherein the centroids of O_2^{2-} dimers occupy the Cl$^-$ positions. The $Pa\bar{3}$ unit cell contains four oxygen dimers, each of which are aligned along different ⟨111⟩ directions. The calculated lattice parameter of the $Pa\bar{3}$ phase is $a = 5.42$ Å (HSE06) and is in good agreement with the experimental value of 5.46 Å.[39] Above 223 K, the O_2^{2-} dimers remain oriented along ⟨111⟩ directions, but in a disordered fashion,[40] and the crystal structure adopts an FCC structure ($a = 5.49$ Å; space group $Fm3\bar{m}$). Given the difficulties associated with simulating a disordered structure, here we have adopted the ordered $Pa\bar{3}$ structure (Figure 2b) for our calculations. This choice is motivated both by the insensitivity of polaron and O_2 dimer migration barriers to dimer orientation (Supporting Information Figure S2) and by our earlier study which showed that the electrical conductivity of amorphous Li_2O_2 was not markedly improved compared to crystalline Li_2O_2.[41]

Table 1 summarizes the calculated bandgaps for Na_2O_2 and NaO_2 as a function of the level of theory. In the case of the

Table 1. Calculated Bandgaps for Na_2O_2 and NaO_2 at Different Levels of Theory[a]

	method	Na_2O_2	NaO_2 ($Pnnm$)	NaO_2 ($Pa\bar{3}$)
present study	GGA	1.76	0	0
	HSE06	4.02	2.04	2.06
	HSE+G_0W_0	6.65	5.56	5.30
previous calculations	B3LYP	4.59[54]	3.30[54]	
	HSE06	2.94[12]	1.11[12]	1.09[12]

[a]In the case of NaO_2, values are reported for both the low temperature (marcasite, $Pnnm$) and intermediate temperature (pyrite, $Pa\bar{3}$) phases.

GGA, a modest bandgap of 1.76 eV is predicted for Na_2O_2, while NaO_2 is predicted to have no gap (i.e., half-metallic behavior based on the density of states (not shown)). In contrast, use of the HSE06 hybrid functional results in the opening of a gap of 4.19 eV for Na_2O_2 and 2.06 eV for NaO_2. The bandgap for Na_2O_2 is similar to that previously reported for Li_2O_2.[20,42] Nevertheless, for both compounds the HSE06 gap is somewhat larger than those reported by Lee et al.[12]
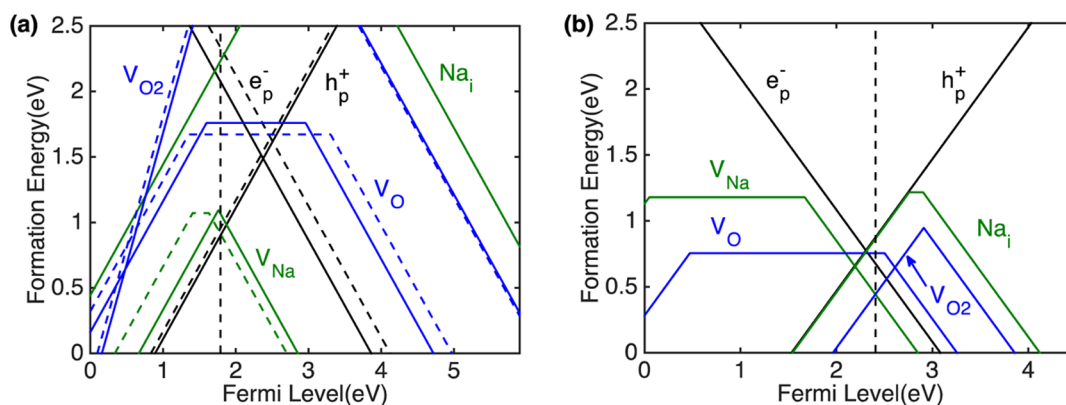
Figure 3. Defect formation energy of the O vacancy (red lines), Na vacancy (green lines), and electron polarons and hole polarons (black lines) obtained using the HSE_α (α = 0.48) hybrid functional in Na_2O_2 (a) and NaO_2 (b). In Na_2O_2 (a), there are two symmetry inequivalent oxygen and sodium sites. The solid line represents the oxygen or sodium defects in the oxygen-rich layer, while the dashed line represents the oxygen or sodium defects in the oxygen-poor layer.

Comparison calculations were also performed on the tetragonal and rock salt structure variants for NaO_2; the data reveal that the bandgap is not very sensitive to the structure type. Non-self-consistent G_0W_0 calculations were performed using wave functions generated by self-consistent HSE06 calculations. Convergence tests were performed with respect to the number of electron states included in the calculation; 512 bands were used for all G_0W_0 calculations. Quasi-particle GW methods have been shown to yield reliable estimates for bandgaps across many different materials.[43] The HSE+G_0W_0 data indicate that both Na_2O_2 and NaO_2 are wide bandgap insulators, with bandgaps of 6.65 and 5.30 eV, respectively. We believe the G_0W_0 calculations provide the best estimate of the true bandgaps of these compounds.

Intrinsic Defects in Na_2O_2. Figure 3 shows the calculated formation energies for O vacancies (V_O), O_2 vacancies (V_{O2}, in which an entire O_2 molecule is removed), Na vacancies (V_{Na}), Na interstitials (Na_i), electron polarons (e_p^-), and hole polarons (h_p^+) as a function of the Fermi level in Na_2O_2 (Figure 3a) and NaO_2 (Figure 3b). The slope of each line in Figure 3 indicates the charge state for the respective defect species: a positive (negative) slope indicates a positively (negatively) charged defect, while a slope of zero indicates a neutral species. Kinks in the curves indicate transitions between charge states; only segments corresponding to the lowest-energy charge states are shown. The zero of the Fermi level corresponds to the valence band maximum (VBM), and the vertical dashed line represents the position of the Fermi level that satisfies charge neutrality.[44]

As shown in Figure 3a, the dominant charged defects in Na_2O_2 are negative sodium vacancies (V_{Na2}^-) and hole polarons (h_{p1}^+) localized on oxygen dimers, with formation energies of 0.91 and 0.90 eV, respectively. (Negative sodium vacancies can occupy two symmetry-distinct Na sites: V_{Na1}^- and V_{Na2}^-. V_{Na1}^- refers to a vacancy in the oxygen-rich layer, while V_{Na2}^- occupies a Na site in the oxygen-poor layer. We find that V_{Na1}^- is 0.15 eV more stable than V_{Na2}^-. Similarly, h_{p1}^+ represents a hole polaron in the oxygen-rich layer, while h_{p2}^+ represents a hole polaron in the oxygen-poor layer; we find h_{p1}^+ to be 0.06 eV more stable than h_{p2}^+.) This behavior is similar to what has been reported in Li_2O_2,[18] wherein the dominant charge-carrying defects were identified as negative lithium vacancies (V_{Li}^-) and hole polarons with formation energies of 0.95 eV. The defects having the next-lowest formation energies

are neutral oxygen vacancies (V_O, E_f > 1.5 eV) and electron polarons (e_p^-, E_f > 2 eV). Using the calculated formation energies as input to eq 1, the equilibrium concentrations of h_p^+ and V_{Na2}^- are estimated to be 1×10^7 cm^{-3}, which are in reasonable agreement with those of Araujo et al., 2×10^8 cm^{-3},[23] whose calculations employed a slightly different value for the mixing parameter, α. As expected, our predicted concentrations are very similar to those for V_{Li}^- and h_p^+ reported in our previous calculations on Li_2O_2,[18] 1×10^7 cm^{-3}. A summary of calculated defect formation energies and concentrations in Na_2O_2 is provided in Table S1 in the Supporting Information. Contrary to some experimental studies on Na_2O_2,[15] we do not find that sodium interstitials are present in high concentrations in Na_2O_2. Indeed, out of a trial set of nine candidate Na interstitial geometries, even the most stable configuration has a high formation energy in excess of 2 eV.

In peroxides and superoxides a hole (electron) polaron consists of a missing (additional) electron localized on an O_2 dimer, resulting in a contraction (extension) of the covalent O−O bond. The localization of a polaron at any given dimer site may be corroborated by examining changes in the O−O bond length, magnetization density, and density of states (DOS) of the system. In Na_2O_2, we observed that the O−O bond length decreases from 1.47/1.48 on the two symmetry-distinct O_2 sites, to 1.31 Å when a hole polaron is present. Analysis of the magnetization density reveals that a magnetic moment $\mu = 1$ μ_B emerges on dimers hosting a hole polaron (Figure 4a), with a characteristic shape of a $\pi_{x,y}^*$ orbital, which is consistent with the presence of an unpaired electron in a superoxide-like O_2^{1-} dimer (Figure 1b). The magnetic moment remains unchanged ($\mu = 0$ μ_B) for other O_2^{2-} ions in the supercell.

The density of states (DOS), Figure 5, provides further information regarding the electronic structure of pristine and defective Na_2O_2. (Note that in Figure 5 the Fermi level ε_F is set to the highest occupied eigenvalue, which is a convention commonly used in first-principles calculations. A more accurate description of the ε_F is given in Figure 3, which accounts for charge neutrality; in this case ε_F is 2.4 (1.8) eV above the VBM for NaO_2 (Na_2O_2).) The DOS for the pristine supercell (Figure 5a) indicates an equal number of spin-up and spin-down states, with full occupation of $\pi_{x,y}^*$ orbitals on the O_2^{2-} dimer. Localization of a hole on the O_2 dimer results in a splitting between the occupied states and unoccupied states of $\pi_{x,y}^*$
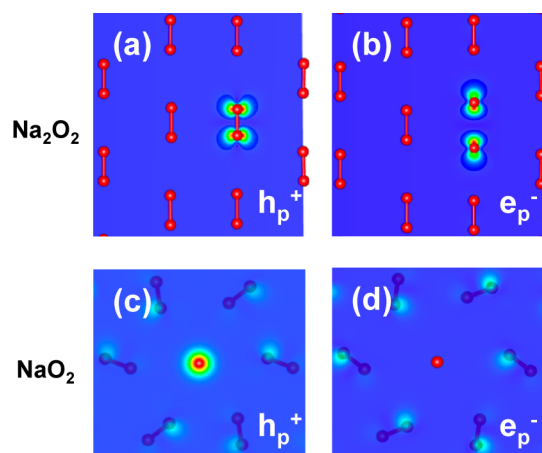
Figure 4. Magnetization density for (a) hole polaron in Na_2O_2, (b) electron polaron in Na_2O_2, (c) hole polaron in NaO_2, and (d) electron polaron in NaO_2. Note that in panels c and d the bond axis of the oxygen dimers is into the plane of the page. The color scheme is set such that blue represents a magnetization density of zero and red corresponds to 0.27 μ_B/bohr^3.

(Figure 5c). This leads to the emergence of a new (empty) state above the Fermi level.

Formation of an electron polaron in Na_2O_2 increases the formal negative charge on the affected peroxide (O_2^{2-}) ion to O_2^{3-}. This electron occupies a σ^* orbital, resulting in a large increase to the O–O bond length from 1.48/1.49 to 2.20/2.29 Å. The presence of the additional electron is also reflected in the DOS (Figure 5b), where a new peak appears below the conduction band minimum (CBM), which is accompanied by the emergence of a new state below the Fermi level and a splitting of occupied spin-up and spin-down channels. This change is concurrent with the emergence of a magnetic moment $\mu = 1\ \mu_B$ on the dimer hosting the additional (unpaired) electron, Figure 4b, which has the characteristic shape of a σ^* orbital.

**Intrinsic Defects in NaO_2.** In NaO_2 the present calculations suggest that the dominant ionic charge carriers consist of three species: negative sodium vacancies (V_{Na}^-), positive oxygen dimer vacancies ($V_{O_2}^{1+}$), and positive sodium interstitials (Na_i^+). These have formation energies 0.44, 0.44, and 0.87 eV, respectively. The formation energies of V_{Na}^- and $V_{O_2}^{1+}$ are approximately 0.46 eV smaller than those of the lowest-energy defects in Na_2O_2, suggesting that the superoxide will support a higher concentration of ionic defects compared to the peroxide. Indeed, the equilibrium concentrations of V_{Na}^- and $V_{O_2}^{1+}$ are on the order of 10^{15} cm^{-3}, which is 8 orders of magnitude higher than for the dominant defects in Na_2O_2 and Li_2O_2. These findings agree qualitatively with the experimental data of Gerbig et al., who found that O_2 vacancies and potassium interstitials were the dominant ionic charge carriers in potassium superoxide.[16] A summary of calculated defect formation energies and concentrations in NaO_2 is provided in Table S2 in the Supporting Information.

Electron polarons (e_p^-) are predicted to be the highest-concentration electronic charge carriers in NaO_2, with formation energies of 0.68 eV (Figure 3b). Somewhat surprisingly, the superoxide also appears to support hole polarons (h_p^+) as minority carriers; the formation energy for hole localization is 0.88 eV, only moderately higher than that for the formation of a localized excess electron.

For an electron polaron in NaO_2 the O–O bond length increases from 1.30 to 1.47 Å, the latter value being very similar to that of peroxide O_2 dimers in Na_2O_2 (1.47/1.48 Å). Moreover, the added electron fills a $\pi_{x,y}^*$ orbital, making that orbital fully occupied, Figure 1c. Subsequently, the magnetic moment on this dimer disappears, while it remains 1 μ_B for the rest of the O_2^{1-} ions in the supercell (Figure 4d). We note that the formation energy of an electron polaron in NaO_2 (0.68 eV) is much lower than in Na_2O_2, 2.07–2.33 eV. This may be explained by the fact that in NaO_2 an electron polaron occupies a $\pi_{x,y}^*$ orbital, whereas in Na_2O_2 it must occupy a higher energy σ^* orbital.
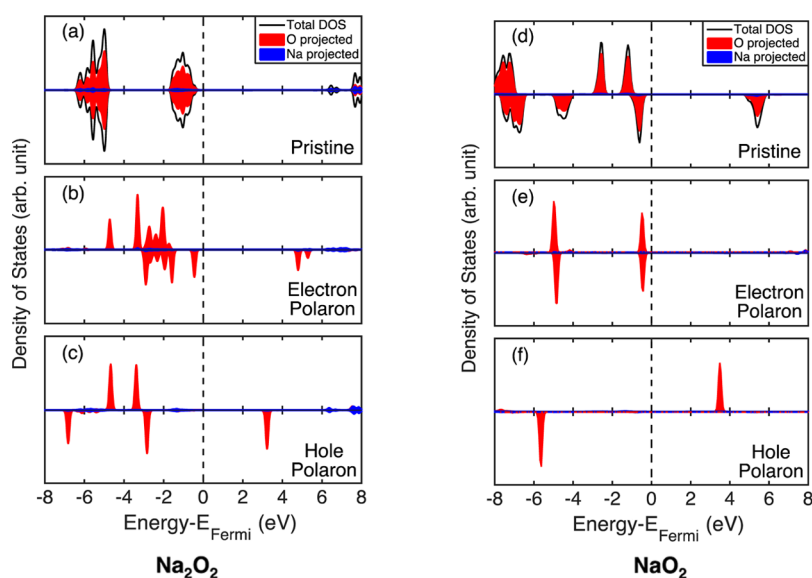
Figure 5. Density of states (DOS) of Na_2O_2 (left panel) and NaO_2 (right panel) calculated using HSE$_\alpha$ ($\alpha = 0.48$). (a, d) DOS for the pristine compounds. (b, e) DOS projected onto an electron polaron cluster. (c, f) DOS projected onto a hole polaron cluster. A cluster is defined as an oxygen dimer and its nearest-neighbor sodium ions.
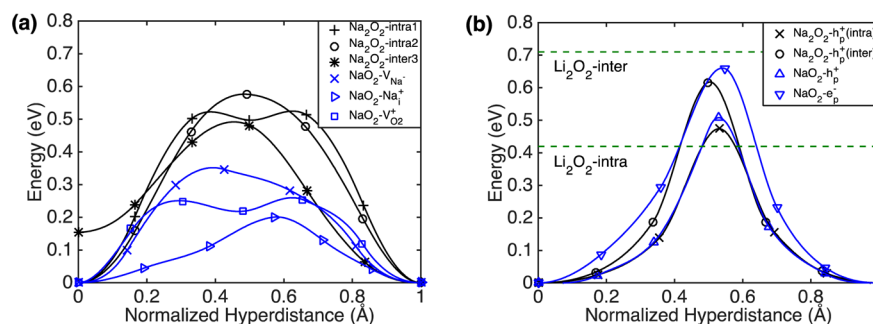
Figure 6. Energy barriers calculated using the NEB method for (a) ionic charge carriers and (b) polarons. Blue curves refer to NaO_2; black curves refer to Na_2O_2. For simplicity, only pathways with barriers less than 1 eV are shown. In panel (a) barriers are plotted for migration of three ionic species in NaO_2: negative sodium vacancies (V_{Na}^-), positive sodium interstitials (Na_i^+), and positive oxygen dimer vacancies ($V_{O_2}^{1+}$). One pathway between nearest-neighbor V_{Na}^-, Na_i^+, and $V_{O_2}^{1+}$ is considered. In Na_2O_2 only V_{Na}^- are relevant, and five distinct pathways were considered between two symmetry inequivalent V_{Na}^- sites. In panel (b), electron polaron (e_p^-) and hole polaron (h_p^+) hopping barriers are compared with those for hole polaron hopping in Li_2O_2 from Radin and Siegel[18] (green dashed lines).

Regarding the nature of hole polarons in NaO_2, similar to what is observed for Na_2O_2, missing electrons localize on O_2 dimers, resulting in a decrease of the O–O bond length from 1.30 to 1.19 Å. Thus, a hole polaron transforms a superoxide dimer, O_2^{1-}, into a neutral gas-like state, O_2^0; this is further supported by the similarity in the O–O bond length for gaseous O_2, 1.21 Å.[45] The magnetic moment on the dimer hosting the hole polaron, $\mu = 2\ \mu_B$, is twice as large as in the peroxide, Figure 4c, and is consistent with gaseous O_2: The trapping of a hole in NaO_2 results in two unpaired electrons in the $\pi_{x,y}^*$ orbital (Figure 1a), with each electron contributing a magnetic moment of 1 μ_B. Consequently, only a spin-down peak can be seen in the DOS of the hole polaron (Figure 5f).

The DOS for Na_2O_2 and NaO_2 share many features upon addition and removal of electrons. For example, in pristine NaO_2, the missing electron in the $\pi_{x,y}^*$ orbitals results in a splitting of the energy levels (Figure 5d). This behavior is very similar to the DOS of an O_2 dimer in Na_2O_2 that hosts a hole polaron, Figure 5c. Similarly, the addition of an electron to NaO_2 converts a superoxide (O_2^{1-}) dimer to a peroxide-like charge state (O_2^{2-}), creating an electron polaron. Note that the DOS for this state, Figure 5e, closely resembles that of pristine Na_2O_2.

Mobilities. The second quantity needed to estimate the conductivity of the Na–O$_2$ discharge phases is the mobility of the predominant (i.e., highest concentration) charge-carrying species. We first consider the mobilities of ionic species. In Na_2O_2, ionic conductivity originates from the migration of negative sodium vacancies, V_{Na}^-. (Since during this process a sodium cation, Na^+, moves counter to the vacancy, one may equivalently consider this mechanism to be vacancy-mediated Na-ion migration.) Energy barriers for seven vacancy migration pathways in Na_2O_2 were calculated using the NEB method. Figure 6a shows the energy profiles for those pathways where the energy barriers are less than 1 eV. We explored both intralayer and interlayer migration pathways. The lowest-energy pathway, "Na_2O_2-intra3," corresponds to migration between a vacant Na site in an oxygen-rich layer (V_{Na1}^-) and an adjacent site in the oxygen-poor layer (V_{Na2}^-). This process has an energy barrier of 0.34 eV relative to V_{Na1}^- and 0.50 eV relative to V_{Na2}^-. Setting E_b to the average of these two values gives a defect diffusion coefficient of 9×10^{-10} cm^2 s^{-1}. The calculated diffusion barriers in Na_2O_2 are in reasonable agreement with that of Araujo et al., 0.50 eV,[23] and are only slightly larger than

what has been reported for the migration of negative lithium vacancies in Li_2O_2, 0.30–0.39 eV.[18,46,47] The slight increase in barriers found for Na_2O_2 may be due to the longer diffusion distance in this phase compared to that of Li_2O_2 (3.02 Å vs 2.60 Å).

Activation energies for the three dominant ionic charge carriers in NaO_2 (V_{Na}^-, Na_i^+, and $V_{O_2}^{1+}$) were also evaluated. The calculations suggest that all of these defects have modest migration barriers (Figure 6a), pathways labeled "NaO_2–V_{Na}^-", "NaO_2–Na_i^+", and "NaO_2–V_{O2}^+") of 0.35, 0.20, and 0.26 eV, respectively, corresponding to diffusion coefficients of 2×10^{-8}, 3×10^{-6}, and 6×10^{-7} cm^2 s^{-1}. The high symmetry of the NaO_2 crystal structure suggests that vacancy migration V_{Na}^- occurs via a single pathway wherein a vacancy migrates from one vertex of a Na-ion octahedron to a nearest-neighbor vertex. This pathway lies close to the octahedron's edge, and slightly below the octahedron faces which meet at the edge joining the relevant vertices. The calculated energy barrier for this process, 0.35 eV (Figure 6a), is slightly smaller than the average barrier for vacancy migration in Na_2O_2. The diffusion of an O_2 vacancy is accompanied by the migration of an O_2 dimer in the opposite direction. The barrier for this process includes the rotation of the dimer as it reorients itself along the [111] direction of the nearest-neighbor site. As previously mentioned, this process exhibits a small barrier of 0.26 eV (Figure 6a), which qualitatively agrees with the experimental data from Gerbig et al., who found that superoxide ions are highly mobile in the heavier alkali-metal superoxides.[16]

Regarding the mobilities of electronic species, Figure 3 indicates that hole polarons are the dominant charged defects in Na_2O_2 while electron polarons are the dominant charged defects in NaO_2. Consequently, activation energies for polaron hopping were calculated for both compounds, Figure 6b using the HSE_α functional. For Na_2O_2, five hole polaron hopping pathways were considered, accounting for the two symmetry inequivalent oxygen dimer sites, as well as intralayer and interlayer hops. In the case of NaO_2, polaron hopping is expected to occur between a given dimer and its 12 nearest-neighbor dimers. Accounting for the different [111] orientations of these dimers, three symmetry-distinct hops are possible. Supporting Information Figure S2 shows that the unrelaxed barriers for these hops are identical, indicating that dimer orientation does not strongly influence the barriers for polaron hopping in NaO_2 (i.e., polaron hopping is isotropic).

Figure 6b shows the polaron hopping barriers for Na_2O_2 (black) and NaO_2 (blue) calculated using the CI-NEB method. We find that the intralayer barrier in Na_2O_2, $E_b^{intra} = 0.47$ eV, is 0.15 eV lower than the interlayer barrier, $E_b^{inter} = 0.62$ eV. This implies that hole polaron hopping is anisotropic, and should be faster in the in-plane directions (i.e., along $[1\bar{1}00]$ or $[11\bar{2}0]$) compared to out-of-plane hopping along $[0001]$. This is similar to what was previously reported in Li_2O_2, where the in-plane barrier (Figure 6b dashed blue line) was 0.42 eV and out-of-plane barrier (dashed green line) was 0.71 eV.[18] Importantly, in NaO_2 the calculated barrier for migration of an electron polaron, 0.66 eV, is higher than that for migration of a hole polaron, 0.51 eV. Therefore, the mobility trend for polaron migration in NaO_2 (i.e., more facile hopping of holes) is the reverse of the stability trend (i.e., electron polarons are more stable).

Conductivity. The conductivity arising from charged defects (polarons or ions) depends on both the concentrations and mobilities of these carriers and may be expressed as

$$\sigma = eC\mu = \frac{Cva^2e^2}{k_BT}e^{-E_b/k_BT} \tag{4}$$

The calculated conductivities for Na_2O_2 and NaO_2 are summarized in Table 2 and compared with prior calculations

Table 2. Calculated Ionic and Electronic Conductivities (S cm^{-1}) for Na_2O_2 and NaO_2 and Their Comparison with Prior Calculations on Li_2O_2[a]

compound	ionic conductivity (S/cm)	electronic conductivity (S/cm)
Li_2O_2	9×10^{-19}	5×10^{-20}
Na_2O_2	5×10^{-20}	1×10^{-20}
NaO_2	$4 \times 10^{-9}/1 \times 10^{-10}$	1×10^{-19}

[a]For ionic conductivities in NaO_2, the first value refers to contributions from positive oxygen dimer vacancies ($V_{O_2}^{1+}$) and the second value refers to contributions from sodium vacancies (V_{Na}^-).

on Li_2O_2. Turning first to Na_2O_2, our calculations suggest that the conductivity of Na_2O_2 is nearly identical to that of Li_2O_2: In both of these compounds the ionic conductivity is similar to the electronic conductivity, with values of approximately 10^{-20} S/cm. The low conductivity values suggest that transport through pristine Na_2O_2 bulk will be limited, unless pathways coupled to microstructural features emerge (surfaces, grain boundaries, and amorphous regions, etc.) Another possibility is that charge will be transported through a liquid phase mechanism involving a soluble superoxide intermediate.[48] Such an intermediate could acquire charge (i.e., be reduced) via electron tunneling through a thin Na_2O_2 film or through adsorption on a portion of the porous carbon support that is not buried by the discharge phase.

Regarding transport in NaO_2, Table 2 shows that the ionic conductivity of this phase is predicted to be significantly higher than in the peroxides. The calculated total ionic conductivity in NaO_2 is 4×10^{-9} S/cm. Most of this conductivity can be attributed to p-type conduction arising from positive oxygen dimer vacancies, with n-type conduction from negative sodium vacancies contributing to a lesser degree. These conductivity values are 9−10 orders of magnitude higher than in Na_2O_2 or Li_2O_2.

The counterbalancing trends in the concentrations and mobilities of hole and electron polarons in NaO_2 results in a nearly equal contribution of these species to the electrical conductivity of NaO_2. Conductivity arising from electron polarons is predicted to be 8.2×10^{-20} S/cm, while for holes the conductivity is about 5.5 times smaller, 1.5×10^{-20} S/cm.

We previously argued that electronic transport was more important than ionic transport in determining the efficiency of Li/O_2 batteries that discharge to crystalline Li_2O_2.[18] This argument was based on the observation that typical cathode support materials, such as carbons, are ion blocking. Consequently, ionic transport would be hindered (except for a transient contribution) due to the inability of Li ions to cross the Li_2O_2/C interface. This scenario also should hold for the Na/O_2 systems considered here. Nevertheless, facile ionic diffusion could facilitate desodiation during charging, resulting in the formation of a substoichiometric $Na_{1-x}O_2$ phase. (Consideration of a desodiation pathway is motivated by earlier studies of the Li−O$_2$ system which proposed delithiation as a mechanism for charging of Li/O_2 cells.[41,49]) If the resulting $Na_{1-x}O_2$ phase exhibited higher electronic conductivity than its stoichiometric parent, then faster ionic conductivity would indirectly contribute to enhanced charge transport. Additional study is needed to test this hypothesis.

We focus the remainder of our discussion on conductivity due to hopping of polarons. It has been suggested that the large size of NaO_2 particles formed during discharge and the low overpotentials observed during charging indicate that this phase should have a higher electronic conductivity than Na_2O_2.[10,11] An earlier experiment also reported that KO_2 had a moderately high electronic conductivity which was comparable to that of copper dust. Nevertheless, the present calculations do not support the notion of high conductivity in NaO_2, given that they predict the superoxide to have a bulk electronic conductivity (10^{-19} S/cm) that is nearly identical to that of sodium peroxide. Our results are consistent with the conclusions reached by Gerbig et al., who measured conductivities of the heavier alkali-metal superoxides (KO_2, RbO_2, and CsO_2.), and found that electronic conductivities were comparable to those of Li_2O_2.[15] A prior study indicated that a conductivity of 10^{-12} S/cm was needed to achieve the performance targets suggested for a practical Li/O_2 cell.[18] According to that analysis, a conductivity of 10^{-19} S/cm (as calculated for NaO_2) would result in an overpotential for the oxygen evolution reaction of approximately 0.4 V, which is significantly larger than what is observed during charging of NaO_2-containing cathodes.[6,8] Therefore, we conclude that a higher electronic conductivity of NaO_2 *cannot* explain the improved performance of cells that discharge to NaO_2.

Which other factors could play a role? Possibilities include conduction pathways that are coupled to microstructural features, such as a higher concentration of polarons at surfaces or grain boundaries.[42,50,51] Deviations from equilibrium conditions—for example during fast discharge—could also result in a higher, nonequilibrium density of charge carriers frozen into the system. Chemical factors may also play a role: A recent study by McCloskey et al.[8] observed that less electrolyte decomposition occurred in a Na−O$_2$ battery during the first galvanostatic discharge−charge cycle. The presence of these side-reaction products has been suggested as a source of overpotentials during OER in Li/O_2 cells.[4,52,53]

4. CONCLUSION

A combination of density functional and quasi-particle calculations have been used to characterize charge transport

in the peroxide and superoxide discharge products commonly observed in Na−O$_2$ batteries. Higher conductivity within the NaO$_2$ phase has been proposed to explain why cells that discharge to NaO$_2$ exhibit much lower charging overpotentials than those that discharge to Na$_2$O$_2$. The present study tests this hypothesis by calculating the intrinsic conductivity of these phases. In so doing, it explores the connection between cell efficiency and the composition of the discharge product. This connection remains poorly understood, as are the mechanisms of charge transport in peroxides and superoxides.

Our calculations reveal that both Na$_2$O$_2$ and NaO$_2$ are electronic insulators, with bandgaps in excess of 5 eV. In the case of sodium peroxide, the transport properties are remarkably similar to those reported previously for lithium peroxide, suggesting a low conductivity on the order of 10^{-20} S/cm.

Compared to the peroxides, transport in superoxides has not been widely explored. The present study reveals that transport in NaO$_2$ has some features in common with the peroxide; nevertheless several important distinctions exist. Similar to Na$_2$O$_2$, NaO$_2$ is predicted to be a poor electrical conductor, wherein transport is limited by sluggish charge hopping between O$_2$ dimers. Different from Na$_2$O$_2$, in NaO$_2$ this transport is mediated by a *combination* of electron and hole polarons. More specifically, conductivity arising from electron polarons is predicted to be 8.2×10^{-20} S/cm, while for holes the conductivity is about 5.5 times smaller, 1.5×10^{-20} S/cm. The mixed contribution to electrical conductivity is due to counterbalancing trends in the concentrations and mobilities of hole and electron polarons in NaO$_2$. Taken together, these data indicate that electronic transport in alkali peroxides and superoxides is governed by the unusual ability of oxygen dimers to adopt three charge states: O$_2^{2-}$, O$_2^{1-}$, and O$_2^0$.

An additional distinguishing feature of the superoxide is its ionic conductivity, which is 10 orders of magnitude larger than the electronic component. The ionic component is comprised primarily of *p*-type contributions from mobile oxygen dimer vacancies, and from n-type contributions from negative sodium vacancies. The mobility of oxygen dimers in the NaO$_2$ lattice is consistent with a recent experimental study by Gerbig et al., who found that superoxide ions are highly mobile in the heavier alkali-metal superoxides.

The limited electronic conductivity predicted for NaO$_2$ suggests that bulk transport within this phase is unlikely to account for the low overpotentials associated with its decomposition during charging in a Na/O$_2$ electrochemical cell. We therefore conclude that the enhanced efficiency observed in cells that discharge to NaO$_2$ must arise from other phenomena, such as a reduction in the extent of electrolyte decomposition or enhanced charge transport through liquid phase processes.

■ ASSOCIATED CONTENT

Ⓢ Supporting Information

Tabulated defect formation energies and concentrations, figures showing unrelaxed migration pathways for various defects, and text describing analysis of structural properties of NaO$_2$ and dielectric constants for Na$_2$O$_2$ and NaO$_2$ used in finite-size corrections. The Supporting Information is available free of charge on the ACS Publications website at DOI: 10.1021/acs.chemmater.5b00285.

■ AUTHOR INFORMATION

Corresponding Author
*E-mail: djsiege@umich.edu.

Notes
The authors declare no competing financial interest.

■ REFERENCES

(1) Bruce, P. G.; Freunberger, S. A.; Hardwick, L. J.; Tarascon, J.-M. Li−O$_2$ and Li−S Batteries with High Energy Storage. *Nat. Mater.* **2011**, *11*, 172−172.

(2) Girishkumar, G.; McCloskey, B.; Luntz, a. C.; Swanson, S.; Wilcke, W. Lithium−Air Battery: Promise and Challenges. *J. Phys. Chem. Lett.* **2010**, *1*, 2193−2203.

(3) McCloskey, B. D.; Scheffler, R.; Speidel, A.; Bethune, D. S.; Shelby, R. M.; Luntz, a C. On the Efficacy of Electrocatalysis in Nonaqueous Li−O$_2$ Batteries. *J. Am. Chem. Soc.* **2011**, *133*, 18038−18041.

(4) McCloskey, B. D.; Bethune, D. S.; Shelby, R. M.; Girishkumar, G.; Luntz, A. C. Solvents Critical Role in Nonaqueous Lithium−Oxygen Battery Electrochemistry. *J. Phys. Chem. Lett.* **2011**, *2*, 1161−1166.

(5) Lu, Y.-C.; Xu, Z.; Gasteiger, H. A.; Chen, S.; Hamad-Schifferli, K.; Shao-Horn, Y. Platinum−Gold Nanoparticles: A Highly Active Bifunctional Electrocatalyst for Rechargeable Lithium−Air Batteries. *J. Am. Chem. Soc.* **2010**, *132*, 12170−12171.

(6) Hartmann, P.; Bender, C. L.; Vračar, M.; Dürr, A. K.; Garsuch, A.; Janek, J.; Adelhelm, P. A Rechargeable Room-Temperature Sodium Superoxide (NaO$_2$) Battery. *Nat. Mater.* **2013**, *12*, 228−232.

(7) Sun, Q.; Yang, Y.; Fu, Z.-W. Electrochemical Properties of Room Temperature Sodium−Air Batteries with Non-Aqueous Electrolyte. *Electrochem. Commun.* **2012**, *16*, 22−25.

(8) McCloskey, B. D.; Garcia, J. M.; Luntz, A. C. Chemical and Electrochemical Differences in Nonaqueous Li−O$_2$ and Na−O$_2$ Batteries. *J. Phys. Chem. Lett.* **2014**, *5*, 1230−1235.

(9) Yadegari, H.; Li, Y.; Banis, M. N.; Li, X.; Wang, B.; Sun, Q.; Li, R.; Sham, T.-K.; Cui, X.; Sun, X. On Rechargeability and Reaction Kinetics of Sodium−Air Batteries. *Energy Environ. Sci.* **2014**, *7*, 3747−3757.

(10) Zhao, N.; Li, C.; Guo, X. Long-Life Na−O$_2$ Batteries with High Energy Efficiency Enabled by Electrochemically Splitting NaO$_2$ at a Low Overpotential. *Phys. Chem. Chem. Phys.* **2014**, *16*, 15646−15652.

(11) Hartmann, P.; Bender, C. L.; Sann, J.; Dürr, A. K.; Jansen, M.; Janek, J.; Adelhelm, P. A Comprehensive Study on the Cell Chemistry of the Sodium Superoxide (NaO$_2$) Battery. *Phys. Chem. Chem. Phys.* **2013**, *15*, 11661−11672.

(12) Lee, B.; Seo, D.-H.; Lim, H.-D.; Park, I.; Park, K.-Y.; Kim, J.; Kang, K. First-Principles Study of the Reaction Mechanism in Sodium−Oxygen Batteries. *Chem. Mater.* **2014**, *26*, 1048−1055.

(13) Kang, S.; Mo, Y.; Ong, S. P.; Ceder, G. Nanoscale Stabilization of Sodium Oxides: Implications for Na−O$_2$ Batteries. *Nano Lett.* **2014**, *14*, 1016−1020.

(14) Khan, A. U.; Mahanti, S. D. Collective Electron Effects of O$_2^-$ in Potassium Superoxide. *J. Chem. Phys.* **1975**, *63*, No. 2271.

(15) GerbigO.*Defect Chemistry in Alkali Peroxides and Superoxides*; Max Planck Institute for Solid State Research: Stuttgart, Germany, 2014

(16) Gerbig, O.; Merkle, R.; Maier, J. Electrical Transport and Oxygen Exchange in the Superoxides of Potassium, Rubidium, and Cesium. *Adv. Funct. Mater.* **2015**, *25*, 2552−2563.

(17) Garcia-Lastra, J. M.; Myrdal, J. S. G.; Christensen, R.; Thygesen, K. S.; Vegge, T. DFT+U Study of Polaronic Conduction in Li$_2$O$_2$ and

Li_2CO_3: Implications for Li−Air Batteries. *J. Phys. Chem. C* **2013**, *117*, 5568−5577.

(18) Radin, M. D.; Siegel, D. J. Charge Transport in Lithium Peroxide: Relevance for Rechargeable Metal−Air Batteries. *Energy Environ. Sci.* **2013**, *6*, 2370−2379.

(19) Varley, J. B.; Viswanathan, V.; Nørskov, J. K.; Luntz, a. C. Lithium and Oxygen Vacancies and Their Role in Li_2O_2 Charge Transport in Li−O_2 Batteries. *Energy Environ. Sci.* **2014**, *7*, 720−727.

(20) Ong, S. P.; Mo, Y.; Ceder, G. Low Hole Polaron Migration Barrier in Lithium Peroxide. *Phys. Rev. B* **2012**, *85*, No. 081105.

(21) Kang, J.; Jung, Y. S.; Wei, S.-H.; Dillon, A. C. Implications of the Formation of Small Polarons in Li_2O_2 for Li-Air Batteries. *Phys. Rev. B* **2012**, *85*, No. 035210.

(22) Gerbig, O.; Merkle, R.; Maier, J. Electron and Ion Transport in Li_2O_2. *Adv. Mater.* **2013**, *25*, 3129−3133.

(23) Araujo, R. B.; Chakraborty, S.; Ahuja, R. Unveiling the Charge Migration Mechanism in Na_2O_2: Implications for Sodium−Air Batteries. *Phys. Chem. Chem. Phys.* **2015**, *17*, 8203−8209.

(24) Kresse, G.; Hafner, J. Ab Initio Molecular Dynamics for Liquid Metals. *Phys. Rev. B* **1993**, *47*, 558−561.

(25) Kresse, G.; Hafner, J. Ab Initio Molecular-Dynamics Simulation of the Liquid-Metal−Amorphous-Semiconductor Transition in Germanium. *Phys. Rev. B* **1994**, *49*, 14251−14269.

(26) Kresse, G.; Furthmüller, J. Efficiency of Ab-Initio Total Energy Calculations for Metals and Semiconductors Using a Plane-Wave Basis Set. *Comput. Mater. Sci.* **1996**, *6*, 15−50.

(27) Kresse, G.; Furthmüller, J. Efficient Iterative Schemes for Ab Initio Total-Energy Calculations Using a Plane-Wave Basis Set. *Phys. Rev. B: Condens. MatterMater. Phys.* **1996**, *54*, 11169−11186.

(28) Kováčik, R.; Werner, P.; Dymkowski, K.; Ederer, C. Rubidium Superoxide: A P-Electron Mott Insulator. *Phys. Rev. B* **2012**, *86*, No. 075130.

(29) Kim, M.; Min, B. I. Temperature-Dependent Orbital Physics in a Spin-Orbital-Lattice-Coupled 2p Electron Mott System: The Case of K. *Phys. Rev. B* **2014**, *89*, No. 121106.

(30) Heyd, J.; Scuseria, G. E.; Ernzerhof, M. Hybrid Functionals Based on a Screened Coulomb Potential. *J. Chem. Phys.* **2003**, *118*, No. 8207.

(31) Krukau, A. V.; Vydrov, O. A.; Izmaylov, A. F.; Scuseria, G. E. Influence of the Exchange Screening Parameter on the Performance of Screened Hybrid Functionals. *J. Chem. Phys.* **2006**, *125*, No. 224106.

(32) Fuchs, F.; Furthmüller, J.; Bechstedt, F.; Shishkin, M.; Kresse, G. Quasiparticle Band Structure Based on a Generalized Kohn-Sham Scheme. *Phys. Rev. B* **2007**, *76*, No. 115109.

(33) Perdew, J.; Burke, K.; Ernzerhof, M. Generalized Gradient Approximation Made Simple. *Phys. Rev. Lett.* **1996**, *77*, 3865−3868.

(34) Makov, G.; Payne, M. C. Periodic Boundary Conditions in Ab Initio Calculations. *Phys. Rev. B* **1995**, *51*, 4014−4022.

(35) Jónsson, H.; Mills, G.; Jacobsen, K. W. *Classical and Quantum Dynamics in Condensed Phase Simulations*; Berne, B. J., Ciccotti, G., Coker, D. F., Eds.; World Scientific: Singapore, 1998.

(36) Henkelman, G.; Uberuaga, B. P.; Jónsson, H. A Climbing Image Nudged Elastic Band Method for Finding Saddle Points and Minimum Energy Paths. *J. Chem. Phys.* **2000**, *113*, No. 9901.

(37) Tallman, R. L.; Margrave, J. L.; Bailey, S. W. The Crystal Structure of Sodium Peroxide. *J. Am. Chem. Soc.* **1957**, *79*, 2979−2980.

(38) Wriedt, H. A. The Na−O (Sodium-Oxygen) System. *Bull. Alloy Phase Diagrams* **1987**, *8*, 234−246.

(39) Carter, G. F.; Templeton, D. H. Polymorphism of Sodium Superoxide. *J. Am. Chem. Soc.* **1953**, *75*, 5247−5249.

(40) Templeton, D. H.; Dauben, C. H. The Crystal Structure of Sodium Superoxide. *J. Am. Chem. Soc.* **1950**, *72*, 2251−2254.

(41) Tian, F.; Radin, M. D.; Siegel, D. J. Enhanced Charge Transport in Amorphous Li_2O_2. *Chem. Mater.* **2014**, *26*, 2952−2959.

(42) Radin, M. D.; Tian, F.; Siegel, D. J. Electronic Structure of Li_2O_2 {0001} Surfaces. *J. Mater. Sci.* **2012**, *47*, 7564−7570.

(43) Shishkin, M.; Kresse, G.; Self-Consistent, G. W. Calculations for Semiconductors and Insulators. *Phys. Rev. B* **2007**, *75*, No. 235102.

(44) Van de Walle, C. G. First-Principles Calculations for Defects and Impurities: Applications to III-Nitrides. *J. Appl. Phys.* **2004**, *95*, No. 3851.

(45) Chambers, C.; Master, S. C.; Holliday, A. K. *Modern Inorganic Chemistry*; Butterworths: London, 1975.

(46) Hummelshøj, J. S.; Blomqvist, J.; Datta, S.; Vegge, T.; Rossmeisl, J.; Thygesen, K. S.; Luntz, a C.; Jacobsen, K. W.; Nørskov, J. K. Communications: Elementary Oxygen Electrode Reactions in the Aprotic Li-Air Battery. *J. Chem. Phys.* **2010**, *132*, No. 071101.

(47) Dunst, A.; Epp, V.; Hanzu, I.; Freunberger, S. a.; Wilkening, M. Short-Range Li Diffusion vs. Long-Range Ionic Conduction in Nanocrystalline Lithium Peroxide Li_2O_2—The Discharge Product in Lithium-Air Batteries. *Energy Environ. Sci.* **2014**, *7*, 2739−2752.

(48) Herranz, J.; Garsuch, A.; Gasteiger, H. A. Using Rotating Ring Disc Electrode Voltammetry to Quantify the Superoxide Radical Stability of Aprotic Li−Air Battery Electrolytes. *J. Phys. Chem. C* **2012**, *116*, 19084−19094.

(49) Kang, S.; Mo, Y.; Ong, S. P.; Ceder, G. A Facile Mechanism for Recharging Li_2O_2 in Li-O_2 Batteries. *Chem. Mater.* **2013**, *25*, 3328−3336.

(50) Radin, M. D.; Rodriguez, J. F.; Tian, F.; Siegel, D. J. Lithium Peroxide Surfaces Are Metallic, While Lithium Oxide Surfaces Are Not. *J. Am. Chem. Soc.* **2012**, *134*, 1093−1103.

(51) Geng, W.; He, B.; Ohno, T. Grain Boundary Induced Conductivity in Li_2O_2. *J. Phys. Chem. C* **2013**, *117*, 25222−25228.

(52) Gallant, B. M.; Mitchell, R. R.; Kwabi, D. G.; Zhou, J.; Zuin, L.; Thompson, C. V.; Shao-Horn, Y. Chemical and Morphological Changes of Li-O_2 Battery Electrodes upon Cycling. *J. Phys. Chem. C* **2012**, *116*, 20800−20805.

(53) Ottakam Thotiyl, M. M.; Freunberger, S. A.; Peng, Z.; Bruce, P. G. The Carbon Electrode in Nonaqueous Li−O_2 Cells. *J. Am. Chem. Soc.* **2013**, *135*, 494−500.

(54) Zhuravlev, Y. N.; Kravchenko, N. G.; Obolonskaya, O. S. The Electronic Structure of Alkali Metal Oxides. *Russ. J. Phys. Chem. B* **2010**, *4*, 20−28.